Icarus ••• (••••) •••–•••

Contents lists available at ScienceDirect

Icarus

www.elsevier.com/locate/icarus

# The detached haze layer in Titan's mesosphere

Panayotis Lavvas *, Roger V. Yelle, Véronique Vuitton [1]

*Lunar and Planetary Laboratory, University of Arizona, 1629 E. University Blvd, Tucson, AZ 85721-0092, USA*

ARTICLE INFO

*Article history:*
Received 13 August 2008
Revised 23 December 2008
Accepted 8 January 2009
Available online xxxx

*Keywords:*
Titan
Atmospheres, structure

ABSTRACT

By comparing observations from the Cassini imaging system, UV spectrometer, and Huygens atmospheric structure instrument, we determine an apparent radius of ~40 nm, an imaginary index <0.3 at 187.5 nm and a number density of ~30 particles $cm^{-3}$ for the detached haze layer at 520 km in Titan's mesosphere. We point out that the detached haze layer is coincident with a local maximum in the measured temperature profile and show that the temperature maximum is caused by absorption of sunlight in the detached haze layer. This rules out condensation as the source of the layer. The derived particle size is in good agreement with that estimated for the size of the monomers in the aggregate particles that make up the main haze layer. Calculations of the sedimentation velocity of the haze particles coupled with the derived number density imply a mass flux 2.7–4.6 × $10^{-14}$ g $cm^{-2}$ $s^{-1}$, which is approximately equal to the mass flux required to explain the main haze layer. Because the aerosol size and mass flux derived for the detached layer agree with those determined for the main layer, we suggest that the main haze layer in Titan's stratosphere is formed primarily by sedimentation and coagulation of particles in the detached layer. This implies that high-energy radical and ion chemistry in the thermosphere is the main source of haze on Titan.

© 2009 Elsevier Inc. All rights reserved.

## 1. Introduction

Titan's thick haze is believed to be a consequence of the vigorous organic photochemistry in its atmosphere, but the chemical processes that lead to haze formation are poorly understood. Some authors have suggested that haze is produced by chemistry in the thermosphere driven by absorption of solar EUV energy (Dimitrov and Bar-Nun, 1999), but others have suggested that the bulk of aerosol production occurs in the stratosphere, driven by absorption of solar FUV radiation (Ferris et al., 2005), especially the chemistry associated with formation of PAHs (Wilson and Atreya, 2003; Lebonnois et al., 2002). Chassefiere and Cabane (1995) and Lavvas et al. (2008b) have argued that both thermospheric and stratospheric sources are important. Recently, Waite et al. (2007) and Coates et al. (2007) have reported the existence of heavy ions and negatively charged aerosols in Titan's thermosphere, proving that some aerosols are created at high altitude. This, along with the rich composition of the ionosphere (Vuitton et al., 2006, 2007), suggests that ion chemistry plays a role in aerosol formation, as is thought to be the case in the interstellar medium (Bohme, 1992). Deciding among these possibilities is difficult on chemical grounds because the chemical pathways to aerosols are not well known and reaction rate data are scarce, but clues to formation mechanisms are present in the haze altitude distribution.

Cassini observations have revealed the presence of a detached haze layer in Titan's mesosphere at an altitude of 520 km, well above the stratosphere. Observations of scattered light made by the Imaging Science Subsystem (ISS) (Porco et al., 2005) reveal a clearly defined layer encircling low and mid-latitude regions. The aerosol layer is also detected in stellar occultation measurements of UV extinction by the UltraViolet Imaging Spectrometer (UVIS) (Shemansky et al., 2005; Liang et al., 2007). We show below that the detached haze layer is coincident with and the likely cause of a local maximum in the temperature profile measured by the Huygens Atmospheric Structure Instrument (HASI) (Fulchignoni et al., 2005). This rules out condensation as the source of the detached haze. Instead, we suggest that the aerosols are formed at higher altitudes by photochemical processes in Titan's ionosphere, becoming visible near 500 km because of the increased number density, caused by the decrease in sedimentation velocity with decreasing altitude, and the increase in scattering and extinction efficiency caused by the aerosol growth through coagulation. Thus, the detached haze layer is a signature of haze formation in Titan's thermosphere.

## 2. Observations

We use observations from three instruments on the Cassini/Huygens mission for our analysis, which are gathered in Fig. 1. The

* Corresponding author. Fax: +1 (520) 621 4933.
*E-mail address:* lavvas@lpl.arizona.edu (P. Lavvas).
[1] Currently at Laboratoire de Planétologie de Grenoble, CNRS/Université Joseph Fourier, Grenoble, France.

0019-1035/$ – see front matter © 2009 Elsevier Inc. All rights reserved.
doi:10.1016/j.icarus.2009.01.004

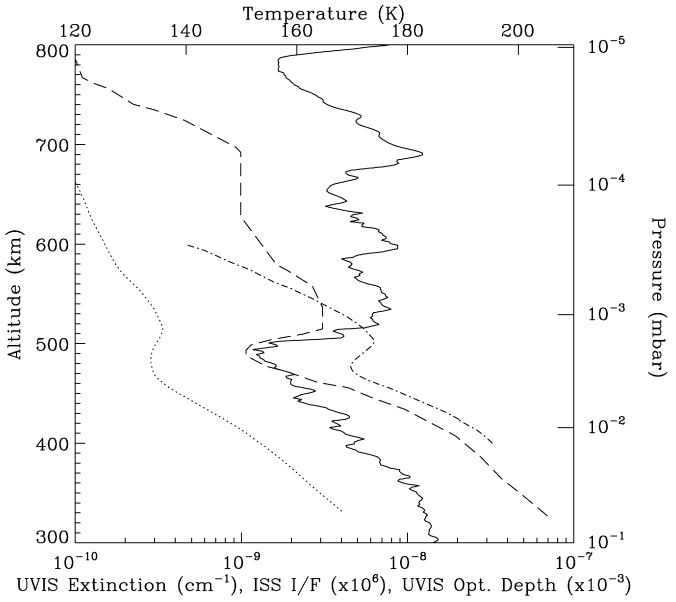


**Fig. 1.** The UVIS retrieved haze extinction profile at 187.5 nm (long-dashed line) based on Liang et al. (2007), the ISS $I/F$ at 338 nm (dash-dotted line; Porco et al., 2005) and the HASI vertical temperature structure (solid line; Fulchignoni et al., 2005) used in the detached haze layer analysis. The dotted line is the UVIS opacity along the line of sight calculated from the retrieved extinction profile.

ISS observations at 338 nm determine the ratio of scattered intensity to incident solar flux, $I/F$. The values shown in the figure are taken directly from Fig. 10 in Porco et al. (2005) for observations made on July 3, 2004 at 10° S latitude. The extinction at 187.5 nm is derived from UVIS observations of the occultation of λ Scorpii by Titan's atmosphere on December 13, 2004 at a latitude of 36° S. The extinction coefficient is derived from the particle density and optical properties published by Liang et al. (2007). Their analysis assumed spherical particles (personal communication with M.-C. Liang). As discussed below, we disagree with Liang et al.'s (2007) interpretation of the observations and therefore we have converted their particle density back to an extinction coefficient, which is more directly related to the observations. The ISS and UVIS observations both show the detached layer near 500 km, but the ISS observations show the layer to be slightly less well defined and at a slightly lower altitude. These differences are due at least in part to the fact that the ISS observations represent the emission rate integrated along the line of sight whereas the UVIS measurements have been inverted to provide the local value of the extinction coefficient. Using the UVIS extinction profile to calculate the opacity along the line of sight shows that the location of peak and trough for the two data sets is the same, hence they are consistent (Fig. 1).

Also shown in Fig. 1 is the vertical temperature profile retrieved by HASI (Fulchignoni et al., 2005) at 10° S latitude on January 14, 2004. The rather small range in latitude and time (compared to the ~7.5 terrestrial years period of a Titan season) suggests that the observations are directly comparable. The measured temperature increases sharply near 509 km, coincident with the UVIS extinction and ISS intensity. This temperature inversion has been detected previously in two ground-based stellar occultation observations that revealed a temperature increase of 15 K over 6 km at an altitude of $515 \pm 6$ km (Sicardy et al., 2006). The two stellar occultations took place within fourteen months suggesting that the inversion layer is not a temporal effect, while the large range of latitudes at which it has been observed suggests that it is not a local phenomenon either. Thus, the detached layer near 520 km is a persistent and global feature in Titan's atmosphere.

Previously, Voyager high phase angle images at 500 nm revealed a detached haze layer near 350 km, covering all latitudes below ~45° N (Rages et al., 1983). Though similar in some respects to the Cassini layer, the Voyager detached layer is located more than 150 km lower. Porco et al. (2005) suggest that the Cassini detached layer could represent a seasonal evolution of the Voyager layer, but this is unlikely. First of all, Voyager images reveal the existence of layers at both 500 and 350 km, though the 500 km layer was at the limit of the Voyager camera sensitivity and, though clearly detected at some latitudes, could not be seen at others (Rages et al., 1983). Moreover, the Voyager and Cassini $I/F$ values are consistent throughout the 400–520 km region. Thus, we conclude that the Cassini detached layer at 520 km is a separate phenomenon rather than a change in the Voyager detached layer.

## 3. Detached haze optical properties

We proceed with the analysis of the detached layer optical properties by making two assumptions: the size distribution of the particles in the layer is narrow enough to be characterized by a mono-dispersed distribution and the shape of the particles can be approximated as spherical. We do not expect the first assumption to significantly affect our conclusions because aerosol size distributions are usually narrow and the optical results will be controlled by the peak size. In addition, we present below the results of an aerosol model that takes into account the size distribution of particles at each altitude. The model allows for the de-convolution of the apparent particle size from the volume-average size, and furthermore supports the second assumption of spherical particles in the detached haze layer.

The observed brightness indicates that the detached haze is optically thin and $I/F$ can be approximated as:

$$\frac{I}{F} = \frac{1}{4} N \pi a^2 Q_{\rm sct} P(\theta) l \tag{1}$$

where $N$ is the local particle density, $a$ the particle radius, $Q_{\rm sct}$ the scattering efficiency, $P(\theta)$ the phase function at scattering angle $\theta$, and $l$ the atmospheric path-length that can be estimated as $l = \sqrt{2\pi RH}$ with $R$ and $H$ the local planetocentric distance and aerosol scale-height, respectively. We neglect illumination of the haze by scattered light from Titan's lower atmosphere because the geometric albedo of 0.05 at 338 nm (Karkoschka, 1994) implies that direct solar illumination dominates. The extinction coefficient is given by $\chi = N\pi a^2 Q_{\rm ext}$, where $Q_{\rm ext}$ is the extinction efficiency. Combining the expressions for the intensity of scattered radiation and extinction leads to:

$$\frac{4(I/F)}{\chi \cdot l} = \frac{[Q_{\rm sct} P(\theta)]^{\rm ISS}}{Q_{\rm ext}^{\rm UVIS}} \equiv \Omega. \tag{2}$$

$Q_{\rm ext}$ and $Q_{\rm sct}$ are functions of wavelength ($\lambda$), particle radius ($a$) and refractive index ($n, k$). The refractive index is a complex number with the real part, $n$, presenting a rather small variability with wavelength, while the imaginary part, $k$, can exhibit significant variation covering many orders of magnitude. In the current calculations we have used $n = 1.65$, the value for tholins at the UVIS and ISS wavelengths (Khare et al., 1984).

The $I/F$ value from ISS observations at 338 nm, phase angle of $\phi = 114°$ ($\theta = 180 - \phi$) and altitude of 520 km is $\sim 5 \times 10^{-3}$, while the UVIS extinction at 187.5 nm is $\sim 3.1 \times 10^{-9}$ cm$^{-1}$. At this altitude $H = 52$ km (Fulchignoni et al., 2005), the atmospheric path-length is $l = 1.0 \times 10^8$ cm and $\Omega = 6.5 \times 10^{-2}$. Examination of the data in Porco et al. (2005) suggests a ~10% variability in $I/F$. Assuming that the uncertainty in $\chi$ at 187.5 nm is of the same order, we conservatively estimate that $\Omega$ must lie between $5 \times 10^{-2}$ and $8 \times 10^{-2}$. Hence, the combination of sizes and optical properties that define the magnitude of $\Omega$ must lie in this range.

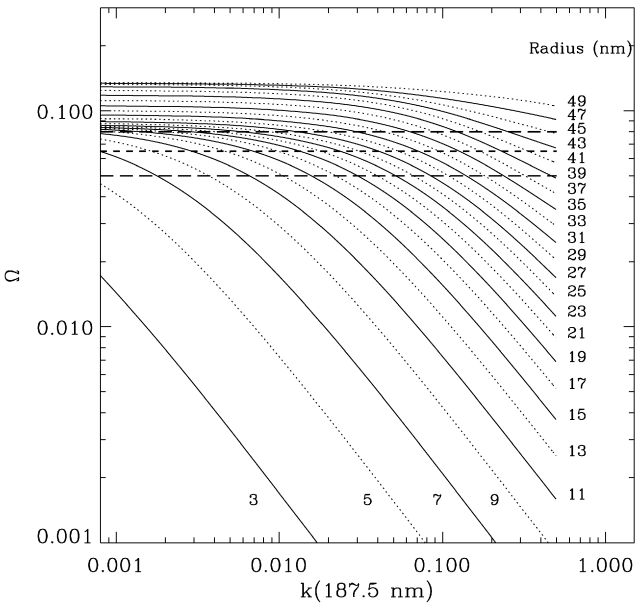


**Fig. 2.** The dependence of parameter $\Omega$ on different values of $k$(187.5 nm) for different particle sizes. The horizontal dashed line corresponds to the value of $\Omega$ defined by the observations and the long dashed lines represent the uncertainty in the observed value.

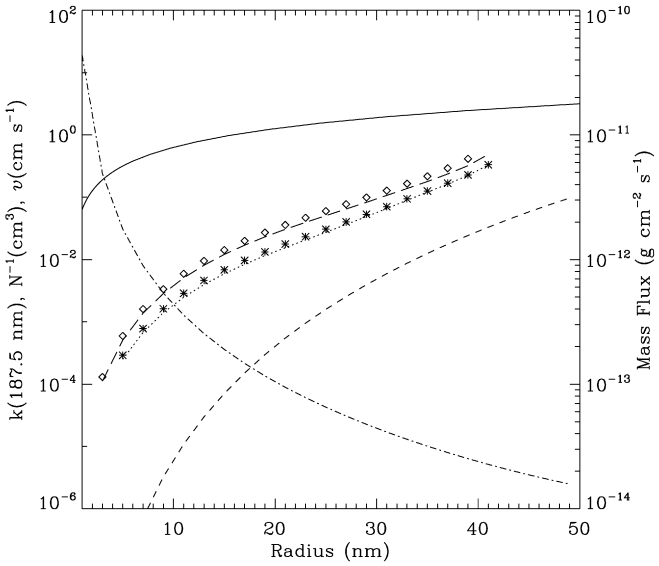


**Fig. 3.** Dependence of settling velocity (solid line), $k$(187.5 nm) (asterisk) and inverse number density (dashed line), on the particle's radius. The sensitivity of the retrieved values of $k$(187.5 nm) on the assumed value of $k$(338 nm) is also shown with the long dashed ($k$(338 nm = 0.3)) and dotted ($k$(338 nm) = 0.01) lines relative to the nominal case of $k$(338 nm) = 0.12 for the asterisk. The diamonds represent the retrieved $k$(187.5 nm) values for the case of larger scale height, discussed in the text. The dash-dotted line is the corresponding mass flux assuming that the aerosols material has a density of 1 g cm$^{-3}$.

The equation used above for the calculation of the path-length assumes an exponentially decreasing aerosol density with altitude. As shown in Fig. 1, the extinction profile is more complex than a simple exponential, but we do not expect this simplification to significantly affect our results. Assuming a scale height $H = 76$ km results in a slightly (due to the square root dependence) larger path length ($1.2 \times 10^8$ cm) and $\Omega = 5.2 \times 10^{-2}$, which is within the uncertainty range of values defined above.

Calculation of the particle scattering properties with Mie theory indicates that $Q_{sct}$(338 nm) and $P(\theta)$(338 nm) are independent of $k$(338 nm) over a large range of values up to ~0.2. On the other hand, $Q_{ext}$(187.5 nm) depends both on $k$(187.5 nm) and $a$; thus, the value of $\Omega$ defines solutions corresponding to pairs of $k$(187.5 nm)–$a$ values. Fig. 2 presents values of $\Omega$ from Mie calculations as a function of $k$(187.5 nm) for a range of $a$. Also shown is the value defined by the observations. We set $k$(338 nm) = 0.12, the value for tholins at this wavelength (Khare et al., 1984). For this case, solutions for $\Omega = 6.5 \times 10^{-2}$ are only obtained for 5 nm $< a <$ 41 nm and consideration of the range of $\Omega$ values indicates that the particle apparent size must be in the range 3 nm $< a <$ 45 nm. The derived value of $k$(187.5 nm) for the detached haze particles is close to (at the large radius limit) or smaller than the value of $k$(187.5 nm) = 0.24 for the particles in the main haze layer (Khare et al., 1984). This suggests that the chemical composition of the detached layer could be different from that of the main haze layer, a conclusion similar to that reached for the particles of the Voyager detached haze layer (Rannou et al., 2000). The latter showed that the relative spectral variation of $k$ between 0.42, 0.5 and 0.58 μm at the Voyager detached haze layer was different from that expected in the main haze layer based on the tholin analogs (Khare et al., 1984), although absolute values of the refractive index could not be retrieved.

Fig. 3 also shows the effect of using different values for $k$(338 nm) to derive values for $k$(187.5 nm) and $a$. Smaller values of $k$(338 nm) do not provide a significantly different solution since $Q_{sct}$(338 nm) and $P(\theta)$(338 nm) are practically independent of $k$(338 nm) for values less than 0.2. The solutions are also quite similar for $k$(338 nm) = 0.3. Values larger than this are unlikely because they would be beyond the range defined by laboratory experiments (Ferris et al., 2005) and would also result in too high $k$(187.5 nm) values (for example, assuming $k$(338 nm) = 0.5 the maximum size retrieved is 38 nm with $k$(187.5 nm) = 0.6).

We calculate the haze number density $N$ for all members of the family of solutions shown in Fig. 2. The inferred densities shown in Fig. 3, range from 36 cm$^{-3}$ for $k$(187.5 nm) = 0.3 and $a = 40$ nm to $3 \times 10^5$ cm$^{-3}$ for $k$(187.5 nm) = 0.0016 and $a = 9$ nm. Assuming an extinction scale height of 76 km only changes the upper limit on $a$ to 39 nm and the associated density to 34 cm$^{-3}$. For clarity of the plot we do not overplot these results in Fig. 3.

With the size and atmospheric density we calculate the sedimentation velocity, also shown in Fig. 3. At these altitudes drag is in the molecular regime and the settling velocity of the particles is given by $v = \alpha a g / u_g \rho_g$ with $g$ the gravitational acceleration, $u_g$ the gas thermal velocity, $\rho_g$ the atmospheric density, and $\alpha$ a numerical coefficient taken equal to 0.7. Our analysis constrains only a family of solutions corresponding to ($k$, $a$) pairs, but particle sizes near the upper end of our range seem far more likely than smaller particles for two reasons: they provide the right heating for generating the observed temperature maximum, and their mass flux is in agreement with the flux allowed by the photochemical processes in the atmosphere. These are discussed hereafter.

Heating of the atmosphere by absorption of sunlight in the detached layer causes the correlation between the haze extinction and temperature shown in Fig. 1. Fig. 4 shows the vertical temperature profile calculated including heating in the detached layer. The temperature is calculated assuming radiative equilibrium and using the non-LTE code described in Yelle (1991). The heating rate is assumed to be a Gaussian in shape, centered at a pressure of 1 μbar with a width of 10 km. The calculated temperature inversion is consistent with that measured by HASI for a peak heating rate in the detached layer of $8.5 \times 10^{-7}$ erg cm$^{-3}$ s$^{-1}$. Fig. 5 shows calculations of the peak heating rate in the detached layer as a function of particle size. The calculations assume optically thin Mie scattering and use tholin optical properties (Khare et al., 1984) in the visible region of the spectrum. The density of haze particles is taken from Fig. 3. A peak heating rate of $8.5 \times 10^{-7}$ erg cm$^{-3}$ s$^{-1}$

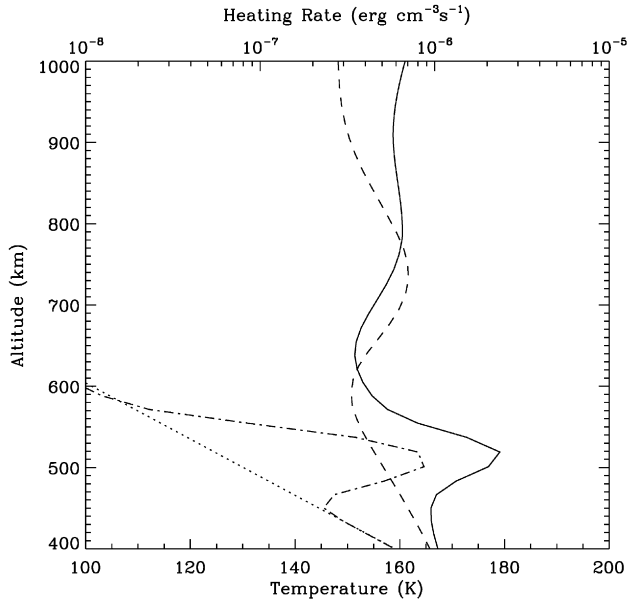


**Fig. 4.** Calculated temperature profiles and aerosol heating rates in Titan's mesosphere for models with and without a detached haze layer. The dot-dashed and dotted lines show the heating rate with and without a detached haze layer; the solid and dashed lines show the corresponding temperature profiles.

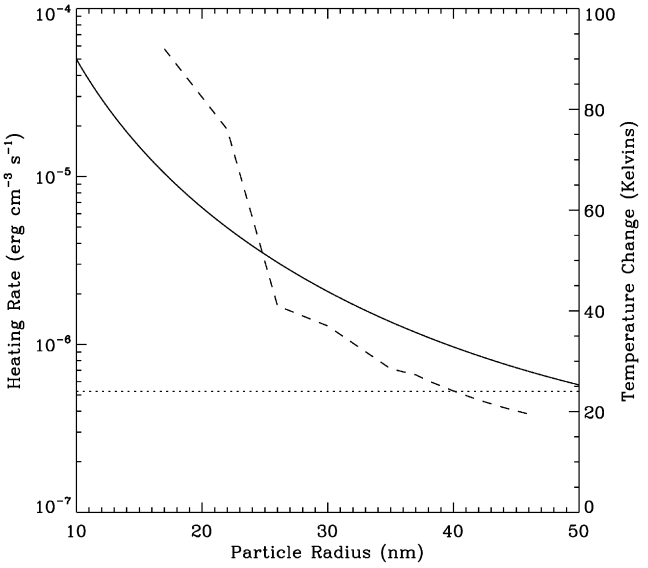


**Fig. 5.** The solid line shows the solar heating rate in the detached layer as a function of the particle radius retrieved by the optical analysis. The dashed line is the calculated temperature increase in the layer corresponding to the heating rate for a given particle size. The dotted line shows the observed temperature increase.

is obtained for a particle radii of 42 nm, but, assuming that the inadequate knowledge of aerosol optical constants and possible departures from radiative equilibrium cause a factor of two uncertainty in the heating rates, we consider that any particle radius greater than 35 nm produces an acceptable solution. Combining this constraint with that determined from the optical analysis presented earlier, we conclude that $a = 35$–$45$ nm for the particles in the detached layer.

Particle radii of ~40 nm are also implied by consideration of the mass flux required to sustain the detached haze layer. The product of aerosol mass, density and settling velocity gives the mass flux, shown in Fig. 3. For $a = 35$, 40, and 45 nm, the mass flux scaled to the surface is 4.6, 3.5, and $2.7 \times 10^{-14}$ g cm$^{-2}$ s$^{-1}$. Larger mass fluxes are difficult to explain on the basis of photochemistry. As discussed below, the total mass production rate above 500 km due to photochemistry is roughly $9 \times 10^{-14}$ g cm$^{-2}$ s$^{-1}$ (Lavvas et al., 2008b; Vuitton et al., 2008), implying that photochemical production of haze in Titan's atmosphere occurs with an efficiency of 30–50%. Particle radii less than ~25 nm would imply that photochemistry leads to aerosol production with 100% efficiency, which is not possible. Thus, consideration of energetics and mass balance both favor particle radii of ~40 nm.

## 4. Previously suggested formation mechanisms

Liang et al. (2007) suggest that the detached layer is caused by condensation of $C_6N_2$ at a temperature minimum near 520 km. The minimum discussed by Liang et al. (2007) is present in the temperature profile derived from the UVIS data but not in the higher resolution and more direct HASI observations. The HASI data clearly show that the haze is coincident with a temperature maximum and consequently the condensation hypothesis must be rejected.

We have also considered a more complicated scenario in which the detached layer is caused by an increase in the density of condensation nuclei near 520 km. This is motivated by the fact that silicate micrometeorites ablate near 500 km (English et al., 1996; Ip, 1990). Recondensation of the refractory vapor creates 'smoke' particles (Hunten et al., 1980) that could serve as condensation nuclei. Pioneer measurements of the dust density near Saturn's region combined with theoretical estimates for the particles velocity distribution, suggest mass fluxes of $\sim 10^{-17}$ g cm$^{-2}$ s$^{-1}$ (Molina-Cuberos et al., 2001), while measurements from the Cassini Dust Analyzer (CDA) suggest a similar magnitude at Titan's location (Srama et al., 2006). These fluxes are ~3 orders of magnitude smaller than the lower limit of our estimated mass flux, so meteorite ablation cannot be the direct cause of the aerosol layer; however, if the ablated meteoritic material reforms 1 nm particles, the implied number flux would be $2.4 \times 10^3$ particles cm$^{-2}$ s$^{-1}$, which is of the right order of magnitude to explain the detached layer.

This hypothesis requires that additional material condense on the meteoritic smoke particles (Hunten et al., 1980). Unfortunately, the main photochemical products on Titan (HCN, $C_2H_2$, $C_2H_6$, etc.) do not condense at the temperature and pressure in the detached layer. The saturation mixing ratios for species present in Titan's mesosphere are shown in Fig. 6. The vapor pressure of each species is calculated assuming the HASI vertical temperature profile (Fulchignoni et al., 2005). The species that come closest to condensing are $H_2O$ and $C_6N_2$. There is some water vapor present from ablation of icy micrometeorites in Titan's atmosphere, but the mole fraction corresponding to saturation vapor pressure of water at 520 km is $1.6 \times 10^{-2}$, many orders of magnitude larger than expected (at 500 km the expected mixing ratio of $H_2O$ is less than $10^{-8}$; Horst et al., 2008). Similarly, the mole fraction of $C_6N_2$ at 520 km is expected to be much smaller than the saturation value of $5 \times 10^{-6}$. The simulated mole fractions of $C_2N_2$ and $C_4N_2$ are close to $10^{-8}$ at 520 km (Lavvas et al., 2008b) and the mole fraction of $C_6N_2$ should be even smaller based on photochemical considerations. Hence, the growth of particles through condensation cannot explain the detached haze layer.

Rannou et al. (2002) suggest that the Voyager detached haze layer is related to advection processes in the atmosphere. In this model, meridional winds transport the haze particles polewards, constraining them at a specific altitude region, before depositing them at the pole, while the upwelling part of the circulation transports large particles from the main haze layer upwards, enhancing in this way the opacity of the detached haze layer. This explanation is unlikely to work for the detached layer at 520 km because sedimentation velocities at these altitudes are much larger. More-

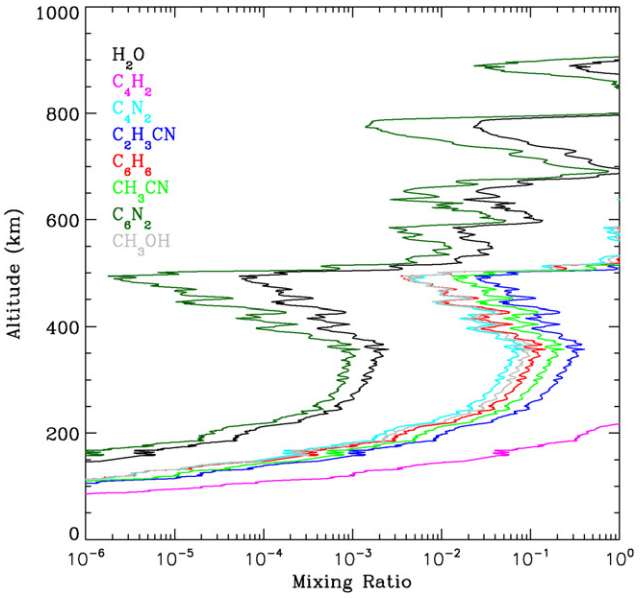


**Fig. 6.** Saturation mixing ratios for plausible condensates in Titan's mesosphere and thermosphere calculated using the HASI vertical temperature profile (Fulchignoni et al., 2005). The vapor pressure data are taken from the NIST database except for $C_6N_2$ which is taken from Saggiomo (1957).

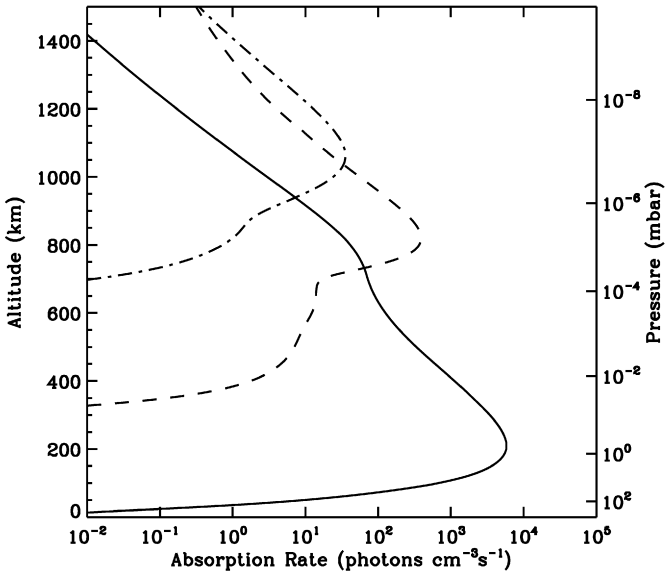


**Fig. 7.** The absorption rate of solar photons versus altitude in Titan's atmosphere. The dot-dashed, dashed, and solid lines represent the integrated flux in the wavelength bands <89.6 nm, 89.6–145 nm, and 145–200 nm, respectively. The first band represents solar ionizing radiation, the second the region over which $CH_4$ is photodissociated into neutral fragments, and the third, absorption by $C_2H_2$, which drives the photocatalytic dissociation of $CH_4$. Calculations assume a solar zenith angle of 60° and are scaled by 0.5 to represent a global-average. The altitude profile of density for absorbing constituents is taken from Yelle et al. (2008) and Vuitton et al. (2008).

over, the detached layer at 520 km is remarkably symmetric and confined within a few km at a constant altitude around Titan (Fig. 10a, Porco et al., 2005). Nevertheless, we can estimate the necessary magnitude of the meridional winds. If meridional winds are responsible for the formation of the detached layer, then their magnitude must be large enough to transport the particles from any latitude to the pole before these settle out of the detached layer region. Otherwise the width of the layer would be variable with latitude and asymmetries would be observed, as is the case for the lower altitude layers observed by ISS (Porco et al., 2005). A 40 nm particle has a settling velocity of $v_S \sim 1\ \mathrm{cm\,s^{-1}}$ at 500 km (Fig. 3), and the characteristic time to fall 20 km is only $2 \times 10^6$ s. Unfortunately, the magnitude of the meridional winds at those altitudes is not known. From the characteristic time for meridional transport, $\tau_H = R/v$ with $R$ the planetocentric distance and $v$ the meridional wind velocity, we can deduce that the latter must be much larger than 150 $\mathrm{cm\,s^{-1}}$ in order to be able to generate the detached layer. The only estimate for the meridional wind magnitude that we have is for the region of the stratospheric zonal jet, where based on CIRS temperature measurements Achterberg et al. (2008) estimated that $v \sim 3\ \mathrm{cm\,s^{-1}}$. If the meridional winds are not significantly enhanced at higher altitudes then they are too small to generate the well-defined detached haze layer. This is something that remains to be verified.

But even if the meridional winds at the location of the detached haze layer are much stronger than those at the stratospheric jet region, the advection solution cannot be a possible explanation for another reason. An important parameter in the dynamical explanation of the detached layer formation is the location of the production region since it is only inside this region where the detached haze layer can be generated (Rannou et al., 2002, 2004). Hence, under the advection description different detached haze layers require different formation altitudes for the aerosols and in the current case of the Cassini detached haze layer this altitude should be close to 500 km. Yet, the large sedimentation velocity retrieved in the detached layer in combination with the inefficiency of condensation or external sources to provide enough mass to generate the detached layer, as shown above, suggests that the aerosols must be formed at higher altitudes. This makes the dynamical solution more difficult to apply. Aerosols formed above 500 km must be produced by the energetic radical and ion chemistry in the thermosphere. Fig. 7 shows calculations of the absorption rate for several UV wavelength bands in Titan's atmosphere. Only chemistry driven by the solar flux below ~145 nm can contribute to the haze seen in the detached layer and this energy is mainly deposited above 700 km. Absorption of longer wavelength solar radiation, which contributes to the photo-catalytic destruction of $CH_4$ and the formation of $C_2H_6$ (Yung et al., 1984), occurs far too deep in the atmosphere to be a factor. The column-integrated photoabsorption rate at wavelengths less than 145 nm corresponds to a globally-averaged mass production rate of $9 \times 10^{-14}\ \mathrm{g\,cm^{-2}\,s^{-1}}$. This value is a factor of 2–3 larger than our estimate of the mass flux in the detached layer, implying that thermospheric chemistry could account for most of the haze in Titan's atmosphere as long as the efficiency is tens of percent.

## 5. Optical illusion scenario

Still, it remains to explain the drop in extinction and $I/F$ just below 500 km. A possible case could be that of an optical illusion. In this scenario the coagulation of the particles that leads to the concentration of their mass into a smaller number of larger size particles, could result in a decrease in their extinction profile, resulting in the apparent detached layer. Aerosol microphysics in this region is quite complex. It is customary to separate coagulation into two distinct phases in which aerosols first grow in a quasi-liquid fashion becoming larger spheres up to a size of ~30–50 nm, after which growth occurs through formation of aggregates of spherical monomers (Bar-Nun et al., 1988; Cabane et al., 1993). The transition from monomer growth to aggregation occurs in this region of the atmosphere (Cabane et al., 1993), but the exact location and the details of the process is not well understood, especially for the initial growth of aggregate particles.

In order to investigate these processes we used the microphysical model described in Lavvas et al. (2008a), which has been ex-

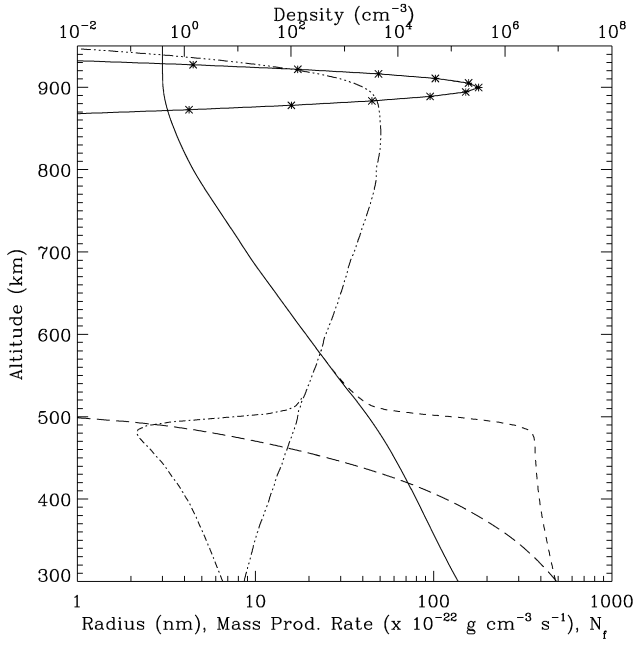


**Fig. 8.** Results of the aerosol model assuming a Gaussian production profile centered at 900 km (solid line with asterisks). The solid and short-dashed lines present the optically-effective radius of the particles averaged between the UVIS and ISS wavelengths, for the two growth processes considered. The apparent size of the particles, presents a sharp increase when these start to coagulate as fractal aggregates (dashed line) close to 500 km, relative to the calculated size when only spherical growth is considered (solid line). Due to volume conservation, the average particle density corresponding to the optically-effective radius, has the inverse behavior (dash-triple dotted line for spheres, dash-dotted line for fractals). The long-dashed line presents the calculated number of monomers in each aggregate, $N_f$.

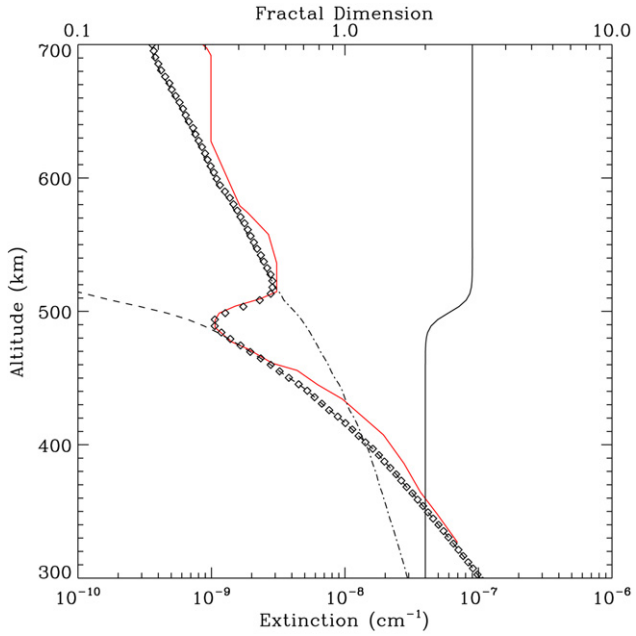


**Fig. 9.** Model results for the extinction by the aerosol particles at 187.5 nm. The dash and dash-dotted lines present the contribution from fractal and spherical particles. These provide a good fit to the extinction profile retrieved by the Cassini/UVIS data analysis at 187.5 nm (Liang et al., 2007—red line) at the altitudes where only spherical (>520 km) or only fractal (<480 km) particles are present. The combined contribution by the two types of particle shapes, at the transition region from spherical to fractal growth (solid line), provides a well-pronounced minimum in the total extinction profile (diamonds), in excellent agreement with the observations. (For interpretation of the references to color in this figure legend, the reader is referred to the web version of this article.)

tended to describe both spherical and fractal particle growth. The model solves the time-dependent continuity equation for particle growth in one dimension, generating the population of different size particles at each altitude. The coagulation of the particles is considered to follow the Brownian or ballistic kernels, depending on the atmospheric pressure, and the necessary adjustments required for the description of the kernels, settling velocities and charge effect between the particles for the case of fractals, were included based on the work of Cabane et al. (1993). The contribution of eddy mixing in the distribution of particles is also included in the calculations with the mixing profile taken from Lavvas et al. (2008b). The model includes 35 size bins that double in volume covering the range between 3 nm and 2 microns. The optical properties of the generated particles are calculated from Mie theory if these are spheres or from the semi-empirical model of Rannou et al. (1999) when they are of fractal structure.

We applied this model in Titan's upper atmosphere focusing on the detached haze layer region. For the particle production we assume a Gaussian profile centered at 900 km and with a column mass production of $6.5 \times 10^{-14}$ g cm$^{-2}$ s$^{-1}$ (Fig. 8). The particles grow as spheres or fractals depending on the fractal dimension, Df (Df < 2 for aggregates and 3 for spheres), which is a free parameter in the model. The transition between spherical to fractal growth allows for a more efficient coagulation between the particles due to the effectively larger collision cross section of the fractal structures. This is shown by the solid and dashed lines in Fig. 8 that represent the optically effective radius of the particles, averaged between the UVIS and ISS wavelengths. At the detached haze peak, the calculated apparent size is in between the size range (35–45 nm) retrieved by our analysis and furthermore the volume-average size of the particles is 30 nm (not shown). The proximity of these two values suggests that our initial assumptions for the optical analysis are valid. Since, under the fractal aggregate growth scenario the particles are larger than in the case of spherical growth, volume conservation requires that the corresponding particle densities exhibit the inverse behavior. This is verified by our calculations, which show a rapid decrease of particle density after the onset of aggregate formation (dash-dotted line) relative to the particle density under spherical growth only (dash-triple dotted line).

Assuming that the particles grow only spherically (Df = 3), results in a good fit to the extinction observed by UVIS at 187.5 nm above the detached haze layer, while the modeled extinction drops faster than the observed extinction at altitudes below the detached layer (Fig. 9). By setting the center of the transition region of spherical to fractal growth at 500 km, the generated fractal particles provide an excellent fit to the observed extinction profile below the detached layer suggesting that the particles present there are indeed of fractal structure (Df < 3). At the same time, the transition from spheres to aggregates, generates a well pronounced minimum in the total simulated extinction, which provides a very good fit to the retrieved detached-layer extinction profile from UVIS (Liang et al., 2007). A local minimum in the extinction profile is also observed in the modeled extinction at 338 nm, although of smaller magnitude (not shown).

The above results suggest that the presence of the detached haze layer is due to the transition in the particle growth process from spherical growth to aggregate growth of fractal structure. We note here that our calculations for the optical properties of the aggregate particles, based on the Rannou et al. (1999) semi-empirical model, correspond to a fractal dimension, Df = 2. The optical behavior of the aggregates for 2 < Df < 3 is not known. To overcome this obstacle we applied an interpolation between the optical properties of spherical particles (based on Mie theory) and the optical properties of fractal aggregates of Df = 2 weighted by the fractal dimension in the transition region (Fig. 9). This approach is sup-

ported by the independent fit of the observations by the model calculations at the regions were only spheres ($z > 520$ km) or only fractals of Df = 2 ($z < 480$) are used.

Finally, the calculated monomer size of the particles forming the fractal aggregates is ~60 nm. We calculate the monomer size at the mid point (Df = 2.5, $z = 500$ km) of the transition region between spherical and fractal growth with Df = 2, which explains the larger size of the monomers relative to the particle size at the detached layer peak. This monomer size is consistent with the 50 nm size retrieved by the DISR measurements (Tomasko et al., 2008), while the corresponding number of monomers in the simulated aggregates reaches to ~1200 in the lower atmosphere (below 200 km) that is also in agreement with the value of 3000 retrieved by DISR. This is an important constraint since the size of the monomers indicates the location of the transition region between spherical to aggregate growth. If the transition was at a much higher altitude than the one used here, the spherical particles would not have enough time to grow to the retrieved monomer size, while if it was at a lower altitude the monomers would be larger and would induce different polarization from that observed by DISR. Of course the above depends on the location of the production profile. Assuming that the production is centered at 600 km, results in a smaller extinction at the spherical-particle growth region above 600 km (and in a reduction in the total extinction) since there is no production at these altitudes any more (and the particles stay for a smaller time in the atmosphere). Yet, the presence of a minimum in the extinction profile at the location of the detached haze layer is a persistent result of the model. If the particle production is below the location of the detached haze layer then the above scenario is not possible. Yet, as discussed above, the production of particles at high altitudes is supported by the detection of large mass negative ions and by the optical analysis of the detached haze layer presented here. A production region at the detached haze layer is also required in the dynamical solution scenario used for the Voyager detected detached layer at 350 km (Rannou et al., 2002). These results provide further support to our suggested model of the detached haze layer formation.

## 6. Discussion

Our analysis of the detached-haze layer from the Cassini/Huygens observations suggests that the transition from spherical to aggregate growth of fractal structure, is the cause for the presence of this feature. Of course the emerging question is why this occurs at the specific altitude. So far the aerosol growth models have described the particle interaction through a sticking efficiency, which is usually parameterized as an empirical number. Nevertheless, this efficiency, which practically conceals the physical and chemical process taking place during the surface interaction between two colliding particles, is a function of the atmospheric conditions, the chemical composition and structure of the aerosols, and of course of the atmospheric gas background. A rigorous theory for the impact of all these parameters is required before a better understanding of the processes defining the shape of the emerging particle, is reached.

Nevertheless, it is interesting to note that the location of the detached haze layer is coincident with the atmospheric region where the main photochemical radicals are depleted (Lavvas et al., 2008b). This could mark the ending of the chemical growth of the particles from the interaction with the atmospheric chemical background and the initiation of a growth mode based only on particle collisions. Furthermore, laboratory measurements (Sekine et al., 2008a) combined with theoretical calculations (Lavvas et al., 2008b; Sekine et al., 2008b) have shown that heterogeneous chemistry on the surface of the haze analogs induce significant changes in the chemical structure of the particle surface, which can have further ramifications in the chemical composition of the atmosphere. Potentially these effects can change the interaction between the colliding particles although the results of their impact are not understood under our current knowledge. Further investigation of the processes defining the growth of the particles is required in order to understand why the transition takes place at this region and how the particles produced at higher altitudes determine the vertical haze opacity in Titan's atmosphere. These issues, along with a more detailed description of the aerosol model presented above will be given in a future publication.

## 7. Conclusions

Our simulation of Titan's haze particle evolution suggests that the presence of the detached haze layer is due to the transition in the growth of particles from spherical to fractal structure. The rapid sedimentation velocity at 520 km implies that the particles in the detached layer will settle to the main layer, raising the possibility that the main haze layer is produced primarily by settling and coagulation of the detached haze layer. Our estimate of ~40 nm for the size of the detached layer particles is also in good agreement with the size ~50 nm inferred for the monomers in the aggregate particles of the main layer (Tomasko et al., 2008). Furthermore, the mass flux of $2.7–4.6 \times 10^{-14}$ g cm$^{-2}$ s$^{-1}$ that we derive for the detached layer is close to the estimates of $0.5–2.0 \times 10^{-14}$ g cm$^{-2}$ s$^{-1}$ for the flux required to produce the main haze layer in the stratosphere (McKay et al., 2001). Because of this close agreement in mass flux, the agreement between the size of the detached haze and main layer monomers, and the fact that the detached layer must sediment to lower altitudes, we suggest that the main haze layer on Titan is formed from sedimentation and coagulation of the detached layer. Thus, the detached layer is not an isolated phenomenon, but the key to understanding aerosol formation for the entire atmosphere. It follows that chemistry in the thermosphere and ionosphere is a primary source for Titan's main haze layer. Given the uncertainty in estimates for the mass flux, we cannot rule out an additional significant source from stratospheric chemistry, but such a source does not appear to be required by the data at the present time.

## Acknowledgments

This work was supported by NASA grants NNG05G085G and NAG5-12699.

## References

Achterberg, R.K., Conrath, B.J., Gierasch, P.J., Flasar, F.M., Nixon, C.A., 2008. Titan's middle-atmospheric temperatures and dynamics observed by the Cassini Composite Infrared Spectrometer. Icarus 194, 263–277.

Bar-Nun, A., Kleinfeld, I., Ganor, E., 1988. Shape and optical properties of aerosols formed by photolysis of acetylene, ethylene and hydrogen cyanide. J. Geophys. Res. 93, 8383–8387.

Bohme, D.K., 1992. PAH and fullerene ions and ion/molecule reactions in interstellar and circumstellar chemistry. Chem. Rev. 92, 1487–1508.

Cabane, M., Rannou, P., Chassefiere, E., Israel, G., 1993. Fractal aggregates in Titan's atmosphere. Planet. Space Sci. 41, 257–267.

Chassefiere, E., Cabane, M., 1995. Two formation regions for Titan's hazes: Indirect clues and possible synthesis mechanism. Planet. Space Sci. 43, 91–103.

Coates, A.J., Crary, F.J., Lewis, G.R., Young, D.T., Waite Jr., J.H., Sittler Jr., E.C., 2007. Discovery of heavy negative ions in Titan's ionosphere. Geophys. Res. Lett. 34, doi:10.1029/2007GL030978. L22103.

Dimitrov, B., Bar-Nun, A., 1999. A model of energy-dependent agglomeration of hydrocarbon aerosol particles and implication to Titan's aerosols. J. Aerosol Sci. 30, 35–49.

English, M.A., Lara, L.M., Lorenz, R.D., Ratcliff, P.R., Rodrigo, R., 1996. Ablation and chemistry of meteoric materials in the atmosphere of Titan. Adv. Space Res. 17 (12), 157–160.

Ferris, J.P., Tran, B., Joseph, J., Vuitton, V., Briggs, R., Force, M., 2005. The role of photochemistry in Titan's atmospheric chemistry. Adv. Space Res. 36, 251–257.

Fulchignoni, M., and 42 colleagues, 2005. In situ measurements of the physical characteristics of Titan's environment. Nature 438 (7069), 785–791.

Horst, S., Vuitton, V., Yelle, R.V., 2008. The origin of oxygen species in Titan's atmosphere. J. Geophys. Res. 113 (E10), doi:10.1029/2008JE003135. E10006.

Hunten, M.D., Turco, R.P., Toon, O.B., 1980. Smoke and dust particles of meteoric origin in the mesosphere and stratosphere. J. Atmos. Sci. 37, 1342–1357.

Ip, W.-H., 1990. Meteoroid ablation processes in Titan's atmosphere. Nature 345, 511–512.

Karkoschka, E., 1994. Spectrophotometry of the jovian planets and Titan at 300 to 1000 nm wavelength: The methane spectrum. Icarus 111, 174–192.

Khare, B.N., Sagan, C., Arakawa, E.T., Suits, F., Calcott, T.A., Williams, M.W., 1984. Optical constants of organic tholins produced in a simulated Titanian atmosphere: From soft X-ray to microwave frequencies. Icarus 60, 127–137.

Lavvas, P.P., Coustenis, A., Vardavas, I.M., 2008a. Coupling photochemistry with haze formation in Titan's atmosphere. Part I: Model description. Planet. Space Sci. 56, 27–66.

Lavvas, P.P., Coustenis, A., Vardavas, I.M., 2008b. Coupling photochemistry with haze formation in Titan's atmosphere. Part II: Results and validation with Cassini/Huygens data. Planet. Space Sci. 56, 67–99.

Lebonnois, S., Bakes, E.L.O., McKay, C.P., 2002. Transition from gaseous compounds to aerosols in Titan's atmosphere. Icarus 159, 505–517.

Liang, M.-C., Yung, Y.L., Shemansky, D.E., 2007. Photolytically generated aerosols in the mesosphere and thermosphere of Titan. Astrophys. J. 61, L199–L202.

McKay, C.P., Coustenis, A., Samuelson, R.E., Lemmon, M.T., Lorenz, R.D., Cabane, M., Rannou, P., Drossart, P., 2001. Physical properties of the organic aerosols and clouds on Titan. Planet. Space Sci. 49, 79–99.

Molina-Cuberos, G.J., Lammer, H., Stumptner, W., Schwingenschuh, K., Rucker, H.O., Lopez-Moreno, J.J., Rodrigo, R., Tokano, T., 2001. Ionospheric layer induced by meteoric ionization in Titan's atmosphere. Planet. Space Sci. 49, 143–153.

Porco, C., and 35 colleagues, 2005. Imaging of Titan from the Cassini spacecraft. Nature 434, 159–168.

Rages, K., Pollack, J.B., Smith, P.H., 1983. Size estimate of Titan's aerosols based on Voyager high-phase-angle images. J. Geophys. Res. 88, 8721–8728.

Rannou, P., McKay, C.P., Botet, R., Cabane, M., 1999. Semi-empirical model of absorption and scattering by isotropic fractal aggregates of spheres. Planet. Space Sci. 47, 385–396.

Rannou, P., Ferrari, C., Rages, K., Roos-Serote, M., Cabane, M., 2000. Characterization of aerosols in the detached haze layer of Titan. Icarus 147, 267–281.

Rannou, P., Hourdin, F., McKay, C.P., 2002. A wind origin for Titan's haze structure. Nature 418, 853–856.

Rannou, P., Hourdin, F., McKay, C.P., Luz, D., 2004. A coupled dynamics microphysics model of Titan's atmosphere. Icarus 170, 443–462.

Saggiomo, A.J., 1957. The dinitriles of acetylenedicarboxylic and polyacetylenedicarboxylic acids. I. Dicyanoacetylene and dicyanodiacetylene. J. Org. Chem. 22, 1171–1175.

Sekine, Y., Imanaka, H., Matsui, T., Khare, B.N., Bakes, E.L.O., McKay, C.P., Sugita, S., 2008a. The role of organic haze in Titan's atmospheric chemistry. I. Laboratory investigation on heterogeneous reaction of atomic hydrogen with Titan tholin. Icarus 194, 186–200.

Sekine, Y., Lebonnois, S., Imanaka, H., Matsui, T., Bakes, E.L.O., McKay, C.P., Khare, B.N., Sugita, S., 2008b. The role of organic haze in Titan's atmospheric chemistry. II. Effect of heterogeneous reaction to the hydrogen budget and chemical composition of the atmosphere. Icarus 194, 201–211.

Shemansky, D.E., Stewart, A.I.F., West, R.A., Esposito, L.W., Hallett, J.T., Liu, Z., 2005. The Cassini UVIS stellar probe of the Titan atmosphere. Science 308, 978–982.

Sicardy, B., and 51 colleagues, 2006. The two Titan stellar occultations of 14 November 2003. J. Geophys. Res. 111, doi:10.1029/2005JE002624. E11S91.

Srama, R., and 40 colleagues, 2006. In situ dust measurements in the inner saturnian system. Planet. Space Sci. 54, 967–987.

Tomasko, M.G., Doose, L., Engel, S., Dafoe, L.E., West, R., Lemmon, M., Karkoschka, E., See, C., 2008. A model of Titan's aerosols based on measurements made inside the atmosphere. Planet. Space Sci. 56, 669–707.

Vuitton, V., Yelle, R.V., Anicich, V.G., 2006. The nitrogen chemistry of Titan's upper atmosphere revealed. Astrophys. J. 647 (2), L175–L178.

Vuitton, V., Yelle, R.V., McEwan, M.J., 2007. Ion chemistry and N-containing molecules in Titan's upper atmosphere. Icarus 191, 722–742.

Vuitton, V., Yelle, R.V., Cui, J., 2008. Formation and distribution of benzene on Titan. J. Geophys. Res. 113, doi:10.1029/2007JE002997. E05007.

Waite Jr., J.H., Young, D.T., Cravens, T.E., Coates, A.J., Crary, F.J., Magee, B., Westlake, J., 2007. The process of tholin formation in Titan's upper atmosphere. Science 316, 870–875.

Wilson, E.H., Atreya, S.K., 2003. Chemical sources of haze formation in Titan's atmosphere. Planet. Space Sci. 51, 1017–1033.

Yelle, R.V., 1991. Non-LTE models of Titan's upper atmosphere. Astrophys. J. 383, 380–400.

Yelle, R.V., Cui, J., Muller-Wodarg, I.C.F., 2008. Methane escape from Titan's atmosphere. J. Geophys. Res. 113 (E10), doi:10.1029/2007JE003031. E1003.

Yung, Y.L., Allen, M., Pinto, J.P., 1984. Photochemistry of the atmosphere of Titan: Comparison between model and observations. Astrophys. J. Suppl. Ser. 55, 465–506.

Please cite this article in press as: Lavvas, P., et al. The detached haze layer in Titan's mesosphere. Icarus (2009), doi:10.1016/j.icarus.2009.01.004